IEEE Access
Multidisciplinary ⋮ Rapid Review ⋮ Open Access Journal

Received December 24, 2021, accepted January 9, 2022, date of publication January 18, 2022, date of current version February 3, 2022.

Digital Object Identifier 10.1109/ACCESS.2022.3144402

AED-Net: A Single Image Dehazing

SARGIS A. HOVHANNISYAN[1], HAYK A. GASPARYAN[1], SOS S. AGAIAN[2] (Fellow, IEEE), AND ART GHAZARYAN[3]

[1]Department of Mathematics and Mechanics, Yerevan State University, Yerevan 0025, Armenia
[2]Department of Computer Science, College of Staten Island (CSI), City University of New York, New York, NY 10314, USA
[3]Research and Development Program, Ympakt LLC, Waltham, MA 02451, USA

Corresponding author: Sargis A. Hovhannisyan (sargis@ympakt.com)

This work was supported in part by the U.S. Department of Transportation, Federal Highway Administration (FHWA), under Contract 693JJ320C000023; and in part by the Research and Development Program of Ympakt.

ABSTRACT In the past decade, significant research effort has been directed toward developing single-image dehazing algorithms. Despite this effort, dehazing continues to present a challenge, particularly in complex real-world cases. Indeed, it is an ill-posed problem because scene transmission depends on unknown and nonhomogeneous depth information. This paper proposes a novel end-to-end adaptive enhancement dehazing network (AED-Net) to recover clean scenes from hazy images. We evaluate it quantitatively and qualitatively against several state-of-the-art methods on three commonly used dehazing benchmark datasets as well as hazy real-world images. Moreover, we evaluated it against the top-scoring methods of the Codalab NTIRE 2021 competition based on the dehazing challenge dataset. Extensive computer simulations demonstrated that AED-Net outperforms state-of-the-art single-image haze removal algorithms in terms of PSNR, SSIM, and other key metrics. Furthermore, it improves image texture, detail edges, boosts image contrast and color fidelity. Finally, AED-Net is more effective under complex real-world conditions.

INDEX TERMS Codalab, Gamma correction, nonhomogeneous haze, region-aware enhancement, single image dehazing.

I. INTRODUCTION

Images captured in hazy or foggy weather conditions can be significantly degraded, rendering the image objects and their features challenging to be identified by imaging systems. The resulting contrast reduction and color shift present a further problem to imaging applications. Liu *et al.* [1] demonstrated that the reduction in detection rate was proportional to the haze density, positing that image dehazing could be a practical solution for image classification, object detection, remote sensing, image or video retrieval, and outdoor surveillance [1]–[4], [50].

Recently, several dehazing algorithms have been developed that rely on additional information, such as depth, polarization, and multiple images [4]–[6], as well as a single image [7]–[12]. Because multiple images or additional physical information are often unavailable, single-image dehazing has received the most attention. Liu *et al.* [26] surveyed algorithms based on the physical model [1]–[3], image enhancement [17], and deep learning (DL) [7]–[16].

The associate editor coordinating the review of this manuscript and approving it for publication was Yongming Li.

A. PHYSICAL MODEL

Considerable progress has been made in understanding the atmospheric scattering model [1]–[3]. Using this model, McCartney [2] provided a theoretical foundation for image dehazing. In particular, the model computes scene radiance based on the global atmospheric light and transmission map. Several studies have focused on assessing atmospheric light. Tan [18] proposed a contrast maximization method for image dehazing based on the key assumption that non-hazy images have higher contrast than hazy images. Most other algorithms estimate the transmission map by empirically leveraging rules for evaluating atmospheric light. He *et al.* [19] used a dark channel prior (DCP) to assess the transmission map based on the assumption that pixel values in haze-free patches are close to zero in at least one color channel. They express the dark channel for image J as

$$J^{dark}(x) = \min_{y\in\Omega(x)}(\min_{c\in\{r,g,b\}} J^c(y)) \tag{1}$$

where c represents one of the three RGB channels and $\Omega(x)$ is a small patch centered on x. Liu *et al.* proposed an exciting intensity projection strategy to estimate the transmission map [48]. It is important to note that prior assumptions in the methods described above may not always work well because

TABLE 1. Comparison of existing methods on different parameters.

	DehazeNet	*AOD-Net*	*GCA-Net*	*FFA-Net*	*FD-Gan*	*RefineDNet*	*DA-Net*	*TBD*	*AED-Net*
No atmosphere estimate			✓	✓	✓	✓	✓	✓	✓
No transmission estimate			✓	✓	✓	✓	✓	✓	✓
Colorfulness		✓			✓		✓	✓	✓
Heavy haze					✓		✓	✓	✓
Real-world domain						✓	✓		✓
Nonhomogeneous haze								✓	✓
Enhanced non-haze edges									✓
Small datasets								✓	✓

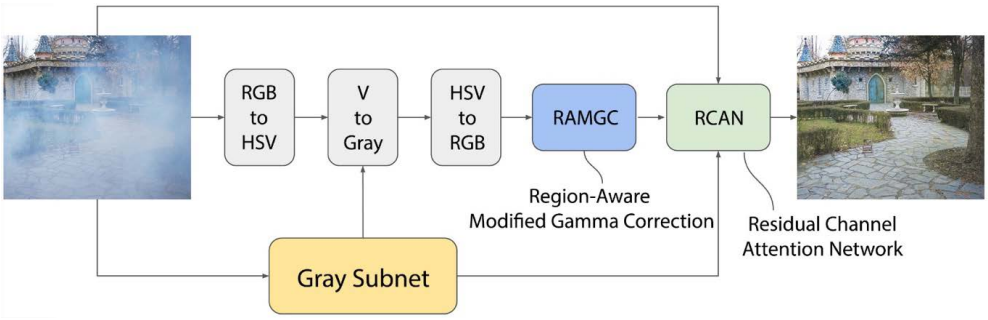

FIGURE 1. Overall architecture of AED-Net.

of inherent limitations in some instances (e.g., dark channel prior assumption does not work well for sky regions.)

B. ENHANCEMENT MODEL

Enhancement-based dehazing does not consider the physical model and improves the image quality by increasing contrast [17]. Huang *et al.* [20] proposed the urban remote sensing haze removal (URSHR) algorithm, which combines phase consistency features, multiscale retina theory [21], and histograms. Chaudhry *et al.* [22] used mixed median and accelerated local Laplacian filtering to dehaze outdoor RGB and remote-sensed images. However, this scheme presents halos in a dehazed image.

C. DEEP LEARNING-BASED MODEL

Convolutional neural networks (CNN) have received considerable attention in recent years due to their success. Several comprehensive surveys of their application in dehazing are available [23], [25], [26]. For example, Gui *et al.* [23] (i) recapped commonly used datasets and loss functions in daytime dehazing tasks, (ii) offered a taxonomy for state-of-the-art DL dehazing algorithms, (iii) introduced core techniques across different methods, and (iv) presented open problems that would inspire further research in image dehazing tasks.

Notably, they conclude that "most papers have discussed the model effect on light and medium haze. Intuitively, the higher the density, the lower is the quality of the dehazed image obtained by the dehazing model." These learning models can be broadly categorized as (a) utilizing the atmospheric scattering model and (b) using an end-to-end approach for estimation. DehazeNet [24] and AOD-Net [7] are good examples of the first category. They used a CNN to estimate the transmission map and atmospheric light. In contrast, many other methods use an end-to-end approach to recover haze-free images without using a physical scattering model. GCA-Net [8] employs smoothed dilated convolution layers to remove gridding artifacts. Qin *et al.* [9] proposed FFA-Net with pixel and channel attention. Shao *et al.* [10] proposed a novel domain-adaptation framework for dehazing tasks.

Another interesting strategy was proposed by Ren *et al.* [49]. They derive three inputs from the original hazy image by applying white balance, contrast enhancement, and Gamma correction. The network computes pixel-wise confidence maps to blend the information derived from the inputs. Most of these techniques perform well in some cases; however, computer simulations show that they have difficulty in real-world situations, for example, working with challenging NTIRE datasets [27], [30], [31], [40], using small-scale training sets, and nonhomogeneous haze. Several excellent methods have been developed for real-world cases tailored to NTIRE datasets.

Sourya *et al.* [11] proposed a fast network for restoring nonhomogeneous haze by aggregating multiple image patches from different image scales. Yu *et al.* [12] introduced a two-branch dehazing network in the Codalab NTIRE 2021 nonhomogeneous dehazing challenge [27]. They proposed a simple approach for nonhomogeneous dehazing via ensemble learning and utilized the Res2Net [28] encoder with ImageNet pre-trained weights. These methods were effective for small training datasets. Despite this remarkable progress,

the performance of these state-of-the-art techniques is influenced by haze-relevant priors or heuristic cues that are not sufficiently efficient. Some properties of the state-of-the-art image-dehazing methods are provided in Table 1.

This article proposes an adaptive enhancement dehazing network (AED-Net) with gray-level projection. Unlike competing methods, the proposed approach combines CNN with concepts from the enhancement model as well as the weak assumption of a dark channel prior [19]. Key differentiating aspects of AED-Net are a unique network structure with novel modules, including (i) a novel region-aware modified Gamma correction (RAMGC) module which has the ability to enhance the edges and distorted colors, (ii) thin and heavy haze enabling model, and (iii) unique integrations of all modules. Finally, the net allows superior haze removal while providing convincing results in a wide range of real-world conditions.

This paper makes several key contributions:

a) An end-to-end convolutional network architecture for single-image dehazing, which does not depend on external information, such as cues acquired from other sources, existing georeferenced models, estimation of the transmission map, assessment of the atmospheric light, or multiple images of the same scene taken under different weather conditions.

b) Novel network modules, including gray-level dehazing (GLD) and RAMGC.

c) Results of extensive computer simulations.

The analysis of these results confirmed that the proposed network outperformed the state-of-the-art single-image haze removal algorithms (AOD-Net [7], DA-Net [10], FDMPHN [11], GCA-Net [8], FD-GAN [13], RefineD-Net [14], FFA-Net [9], and Wavelet U-Net [15]) on real-world images, including benchmark datasets such as I-Haze [31], O-Haze [30], and NH-Haze2 from Codalab NTIRE 2021 competition [27].

The remainder of this paper is organized as follows. Section II provides a detailed description and analysis of the AED-Net architecture. Section III presents the experimental results, including an ablation study and comparison with other dehazing methods. Finally, Section IV concludes the study.

II. PROPOSED METHOD

This section introduces the overall AED-Net architecture and provides details of its three main components: gray-level dehazing, residual channel attention, and region-aware modified Gamma correction modules. In addition, it describes the loss functions for training the network.

A. OVERVIEW OF THE NETWORK ARCHITECTURE

The presented AED-Net architecture contains three essential parts: (i) estimation of a global high-level dehaze map for a single channel without haze-relevant features, (ii) enhancement of non-haze edges and reconstruction of colors affected by haze and (iii) augmentation of the final result with fine detail information. As illustrated in Fig. 1, the input image is first passed to the GLD module to produce a single-channel dehazed output. Although this module performs well at the gray level, the output lacks color and fine features, as expected from its structure (Fig. 2(a)). Next, we fuse the gray-level channel result with the input image using the color space conversion technique, inspired by [51]. First, the initial image is converted into the HSV color space, and then the V channel is replaced by the gray-level dehazed output. The results are then converted back to the RGB space. Next, we perform a novel region-aware Gamma correction (Fig. 3(a)) to enhance the edges and distorted colors, as detailed in Section C. Finally, we employ the residual channel attention network (RCAN) [29] to re-introduce fine features from the original Image (Fig. 2(b)).

B. GRAY LEVEL DEHAZING

Haze is not uniformly distributed within the RGB channels [27]. For instance, the haze density in the blue channel is much higher than in the red channel. We posit that single-channel prediction would present a less challenging task than utilizing three channels simultaneously. Our experimental results validate this assumption. GLD has an encoder-decoder structure with a Res2Net encoder inspired by [28]. The encoder module loads the ImageNet pre-trained parameters to achieve faster convergence, mitigate overfitting on small datasets, and extract more robust features. We used two branches for the thin and heavy haze to construct the decoder. The main structures of the two units are similar. They both utilize upsampling PixelShuffle [32] modules with convolution layers followed by channel attention and pixel attention layers [9]. Furthermore, we used dilated convolutional layers with larger kernel sizes to enlarge the receptive field for a heavy haze branch. We used a dark channel prior (DCP) [19] as a weight map to fuse the branches, assuming that if the pixel value on the dark channel is high, there is a high probability that it would be a hazy pixel. In other words, we interpret the dark channel as a haze probability map. Fusion was performed as follows:

$$O = O_h \cdot DC + O_l \cdot (1 - DC) \tag{2}$$

where O_h is the output of heavy haze branch decoder, O_l is the output of the thin haze branch decoder, O is the resulting image after fusion, and DC is the dark channel.

C. REGION AWARE MODIFIED GAMMA CORRECTION

The color distribution of hazy images can vary based on the haze source (poor weather, traffic, industry, etc.) and its type (thin haze, heavy haze, dark haze, etc.). This section proposes a novel image-enhancement approach for adapting the color distribution of haze and highlighting the edges. A Gamma correction strategy was proposed by Liu *et al.* [33] as a pre- processing step. Although this approach can improve the overall brightness and shift the color distribution globally, it has certain limitations: (i) a global optimal Gamma parameter should be determined for an individual image as

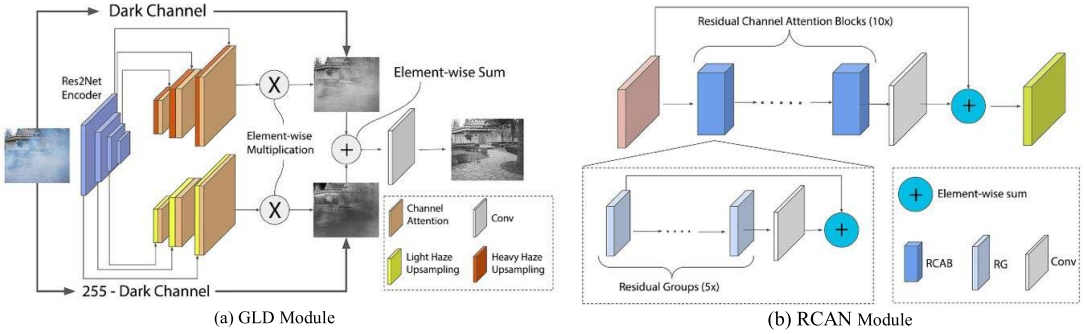

(a) GLD Module (b) RCAN Module

FIGURE 2. GLD module (a) and RCAN module (b).

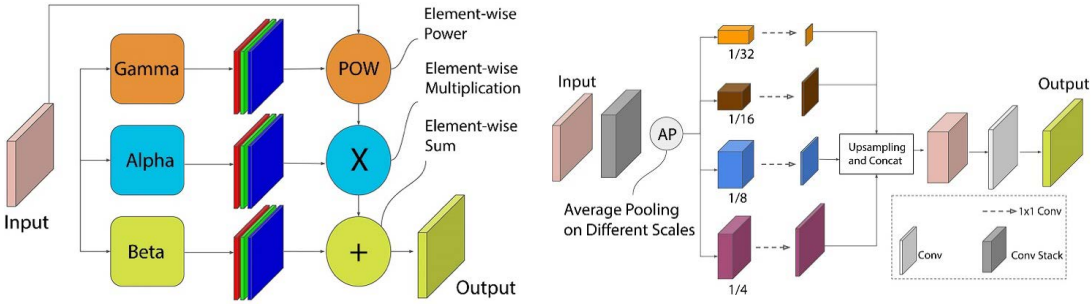

(a) RAMGC Module (b) Enhancement Module

FIGURE 3. RAMGC module (a) consisting of three enhancement blocks, where each block Gamma, Alpha, Beta has architecture (b).

the haze type can vary across images, (ii) it does not effectively address different regions of the image because the haze can be spatially nonhomogeneous, and (iii) preferably, it could be adjusted to highlight edges. We aimed to build a network that would perform well for different haze types and spatial distributions. We propose a Gamma map with an individual Gamma parameter for each pixel per channel, based on the global and local properties of the input image. Furthermore, we created a block that learns to output a Gamma map depending on the haze type and location. Finally, we introduced two additional feature maps to enlarge the transformation space. The module outputs three feature maps and transforms the input image X as follows:

$$X^C_{enhanced} = \alpha(X^C)^\gamma + \beta \tag{3}$$

where α, β, and γ are the three corresponding outputs, $C \in \{R, G, B\}$ is the color channel index, and X^C is the color channel of the input. This module uses pyramid pooling blocks to ensure that features from different scales are embedded in the final result. As shown in Fig. 3 (a), we used the same image enhancement block described in [34] with different (non- shared) weights for each output map. This enabled us to enlarge the receptive field and obtain region-aware maps (Fig. 3 (b)). A detailed description of the enhancement block can be found in [34].

D. RESIDUAL CHANNEL ATTENTION

This module, shown in Fig. 2 (b), aims to fuse globally dehazed high-level details with low-level features from the hazy input image that are lost during the preceding transformations. We used residual channel attention blocks introduced in the super-resolution problem [29], each containing respective convolutional layers and channel attention modules. This design is less sensitive to gradient vanishing due to the residual connections. Channel attention is used to highlight the required feature maps. Furthermore, this subnet avoids employing downsampling and upsampling to preserve fine features.

E. DISCRIMINATOR AND LOSS FUNCTIONS

1) DISCRIMINATOR

We utilized a discriminator network for adversarial loss to obtain realistic images. It has a straightforward structure with a few 3×3 kernel-size convolutions followed by leaky ReLU activations with 0.2 parameters and batch normalization. The output dimensions of the convolutional layers are 64, 128, 256, and 512. The final layers perform 2D adaptive pooling, followed by convolution with a kernel size of 1. The last layer generates an output vector with a length of 1024. A sigmoid function was used, and the result was averaged to obtain the output probability of the image being real.

2) LOSS FUNCTIONS

We employ a linear combination of four loss functions, smooth L1 [35], MS-SSIM [38], perceptual [36], [37], and adversarial [39], to balance the different losses:

$$L = \gamma_1 L_{l1} + \gamma_2 L_{MS-SSIM} + \gamma_3 L_{perc} + \gamma_4 L_{adv} \quad (4)$$

where γ_1, γ_2, γ_3 and γ_4 are the hyperparameter coefficients.

III. EXPERIMENTS

This section evaluates AED-Net and compares the results qualitatively and quantitatively with those of existing state-of-the-art dehazing methods on benchmark datasets and real-world images (Figs. 4-6.)

A. DATASETS

We chose the following three small benchmarking datasets for training and evaluating our method.

1) I-HAZE

The I-HAZE dataset [31] contains 35 PNG image scenes that correspond to indoor environments, with objects of different colors and varying spatial features. Haze was generated using professional generators (LSM1500 PRO 1500 W) of dense vapor in a controlled indoor environment. The set contains the ground truths corresponding to haze-free images of the same scene. Five images were used for validation, and another five were used for testing.

2) O-HAZE

The O-HAZE dataset [30] was derived from 45 PNG images with and without haze. The acquisition process was similar to that for the I-HAZE dataset. A special hazy liquid with a higher density was chosen to simulate the effect of water haze over larger distances. Similarly, five validation images and five for the test sets were selected.

3) NH-HAZE2

NH-Haze2 was introduced for the Codalab NTIRE 2021 image-dehazing challenge [27]. It consists of 35 hazy PNG images and their corresponding ground truths. It contains real outdoor scenes with nonhomogeneous haze generated using two professional haze machines generating vapor particles with a diameter of 1-10 microns, typical of atmospheric haze. Similarly, we used five images for validation and five for the test sets. The last five images were chosen for testing in the absence of an official test set. We also augmented our training dataset with the data introduced during the NTIRE2020 dehazing challenge (NH-Haze) [40]. We compared our results with Codalab NTIRE 2021 image dehazing challenge top-scoring methods, namely, the first-, third-, and fifth-place winners who provide public code, which allowed us to reproduce their results (Table 4).

B. IMPLEMENTATION DETAILS

The training images were cropped to 256 × 256 random patches, and our data augmentation method provided 90°, 180°, and 270° of random rotation, horizontal, and vertical flipping. This type of augmentation and cropping allowed us to train the model for several epochs in order to achieve better convergence. Initially, the gray module was trained with a higher learning rate (10^{-3}) compared with other parts of the network (10^{-6}). The same loss functions described previously (Section II) were used on both the output of the GLD module (one channel) and the overall network's output (three channels). To calculate perceptual loss, we stack the output three times to obtain the input image in appropriate dimensions because the output of the gray subnet has one channel, whereas VGG [37] takes three channels as an input. After achieving a degree of convergence for the gray-level module, the learning rate was set to 10^{-4} for all, and the learning rate scheduler was set to 200, 500, 1000, and 2000 epochs with a multiplication coefficient of 0.5. We determine the loss functions' hyperparameters as $\gamma_1 = 1$, $\gamma_2 = 0.5$, $\gamma_3 = 0.01$, and $\gamma_4 = 0.0001$ using extensive computer simulations. All experiments are performed on NVIDIA RTX 3080 GPU.

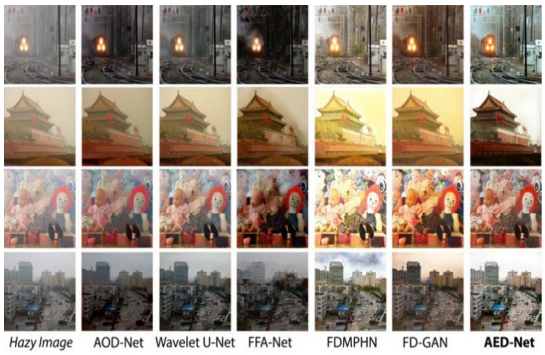

FIGURE 4. Qualitative comparisons of AED-Net on real-world images.

C. QUALITATIVE EVALUATION

Figs. 4-6 show a qualitative comparison of AED-Net with the other methods. As shown in Fig. 6 (a), for the indoor images, DA-Net [10] and FD-GAN [13] managed to clean haze and recover colors in some parts of the image. They failed to remove the heavy haze in the first row or recover the color of the wall in the second one. Although GCA-Net [8] succeeded in removing heavy haze in the first row, it reduced brightness and lost some of the colors. Similar brightness and contrast problems were present in the output produced by FFA-Net [9]. AOD-Net [7] and Wavelet U-Net [15] had similar results. They preserved the color better but retained a thin layer of haze. On the other hand, AED-Net removed both thin and heavy haze layers and maintained the colors consistent with the ground truth. A similar outcome can be observed in the outdoor images shown in Fig. 6 (a). Because the haze has a blue tint in this dataset, almost all methods failed to restore the original colors. The output has either a blue layer or darker regions. DA-Net succeeded in restoring colors consistent with the ground truth; however, it did not remove the haze from the first image or restore the natural sky colors in the third row. We continue to observe similar problems when the haze

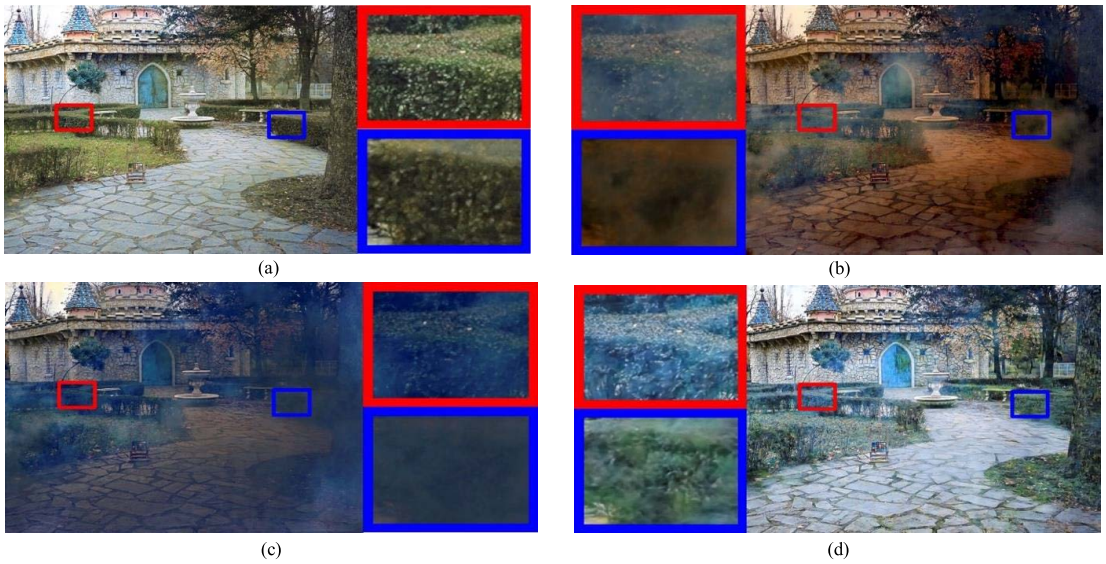

FIGURE 5. This figure shows our ability to recover both high-level and low-level feature features as well as colors (a) compared with DA-Net (b), GCA-Net (c) and DMPHN (d).

TABLE 2. Quantitative comparison of AED-Net with other state-of-the-art methods.

	AOD	DA	FDMPHN	FD_GAN	RefineDNet	FFA	GCA	Wavelet	AED-Net
O-Haze Test Dataset									
	Avg / Std	*Avg / Std*	*Avg / Std*	*Avg / Std*	*Avg / Std*	*Avg / Std*	*Avg / Std*	*Avg / Std*	*Avg / Std*
LPIPS$_{Alex}$	0.434 / 0.07	0.354 / 0.04	0.293 / 0.05	0.364 / 0.05	0.339 / 0.05	0.483 / **0.03**	0.365 / 0.04	0.528 / 0.05	**0.264** / 0.04
PSNR	17.86 / 1.96	18.66 / 1.63	19.763 / 2.81	18.07 / 1.75	16.13 / 1.66	22.12 / 1.61	16.462 / **1.49**	16.47 / 1.63	**25.56** / 1.69
SSIM	0.646 / 0.09	0.77 / 0.04	0.745 / 0.06	0.73 / 0.04	0.716 / 0.04	0.768 / 0.04	0.702 / 0.05	0.656 / 0.04	**0.845** / **0.03**
FSIM	0.770 / 0.04	0.826 / 0.02	0.8229 / 0.02	0.812 / 0.01	0.8141 / 0.02	0.765 / 0.02	0.829 / 0.02	0.795 / 0.02	**0.849** / **0.01**
VIFP	0.268 / 0.05	0.326 / 0.03	0.298 / 0.03	0.289 / 0.03	0.296 / 0.04	0.235 / 0.04	0.314 / 0.03	0.278 / 0.03	**0.349** / **0.03**
I-Haze Test Dataset									
LPIPS$_{Alex}$	0.364 / 0.08	0.36 / 0.09	0.464 / 0.09	0.357 / 0.08	0.373 / 0.09	0.48 / 0.05	0.34 / 0.08	0.39 / 0.07	**0.31** / **0.08**
PSNR	15.41 / 2.45	16.26 / 2.93	14.868 / 3.16	17.61 / 3.21	14.1 / 1.95	11.81 / 2.79	12.75 / **1.83**	14.54 / 2.37	**20.75** / 2.8
SSIM	0.759 / 0.06	0.791 / **0.04**	0.694 / 0.04	0.785 / 0.06	0.73 / 0.05	0.65 / 0.08	0.74 / 0.08	0.788 / 0.05	**0.872** / 0.06
FSIM	0.758 / 0.05	0.8 / 0.04	0.743 / 0.03	0.791 / 0.04	0.78 / 0.04	0.72 / 0.04	0.78 / 0.04	0.797 / 0.04	**0.823** / **0.03**
VIFP	0.26 / 0.07	0.33 / 0.06	0.289 / 0.06	0.302 / 0.06	0.289 / 0.07	0.2 / 0.06	0.28 / 0.07	0.295 / 0.07	**0.367** / **0.05**
NH-Haze2 Test Dataset									
LPIPS$_{Alex}$	0.501 / 0.09	0.432 / 0.07	0.336 / 0.07	0.506 / 0.07	0.433 / 0.08	0.519 / 0.09	0.422 / 0.09	0.598 / 0.08	**0.201** / **0.05**
PSNR	12.42 / 0.96	12.171 / 1.86	16.283 / 1.62	10.474 / **0.56**	11.865 / 1.44	20.4 / 0.87	12.661 / 2.66	11.578 / 0.56	**24.653** / 1.12
SSIM	0.613 / 0.09	0.765 / 0.09	0.745 / 0.05	0.592 / 0.05	0.694 / 0.09	0.806 / 0.11	0.666 / 0.12	0.595 / 0.08	**0.8681** / **0.03**
FSIM	0.745 / 0.05	0.777 / 0.04	0.816 / 0.04	0.684 / 0.03	0.793 / 0.05	0.698 / 0.06	0.791 / 0.05	0.725 / 0.04	**0.877** / **0.03**
VIFP	0.286 / 0.06	0.306 / 0.05	0.355 / 0.06	0.203 / **0.02**	0.33 / 0.07	0.232 / 0.07	0.331 / 0.09	0.263 / 0.05	**0.401** / 0.06

is nonhomogeneous, as shown in Fig. 6 (b). Virtually all methods are unable to completely remove haze because of its heterogeneity. Only FDMPHN [11] removed the haze but retained artificial colors on hazy parts. In contrast, AED-Net has discernible advantages, as shown in Fig. 5, in preserving edges, texture, contrast, brightness, and other image features. Fig. 4 demonstrates the generalizability of AED-Net to real-world images using four canonical hazy images. Some haze remains for AOD-Net, Wavelet U-Net, and FFA-Net. Furthermore, the resulting images lack brightness, and the sky regions have non-natural colors in the case of the second image. Similarly, a loss of brightness can be observed for the third and fourth images, which have many non-natural properties. In the case of FDMPHN and FD-GAN haze is removed. However, certain color distortions are brighter than the original color. Finally, the sky regions appear unnatural. AED-Net successfully removed almost all haze while preserving the essential properties of the images. Finally, the colors are not distorted, and the images appear natural, including consistent colors in the sky regions.

D. QUANTITATIVE EVALUATION

We adopted five image quality metrics for our quantitative analysis [41]–[47]: (i) peak signal-to-noise ratio (PSNR), (ii) structure similarity index measure (SSIM) [41], (iii) feature similarity index measure (FSIM) [42] due to its capacity to reflect the properties of the human visual system (HVS) for perceiving an image based on its fine features, (iv) visual information fidelity (VIF) [43], which uses natural scene statistics and the notion of image information extracted by HVS, and a perceptual metric LPIPS [44].

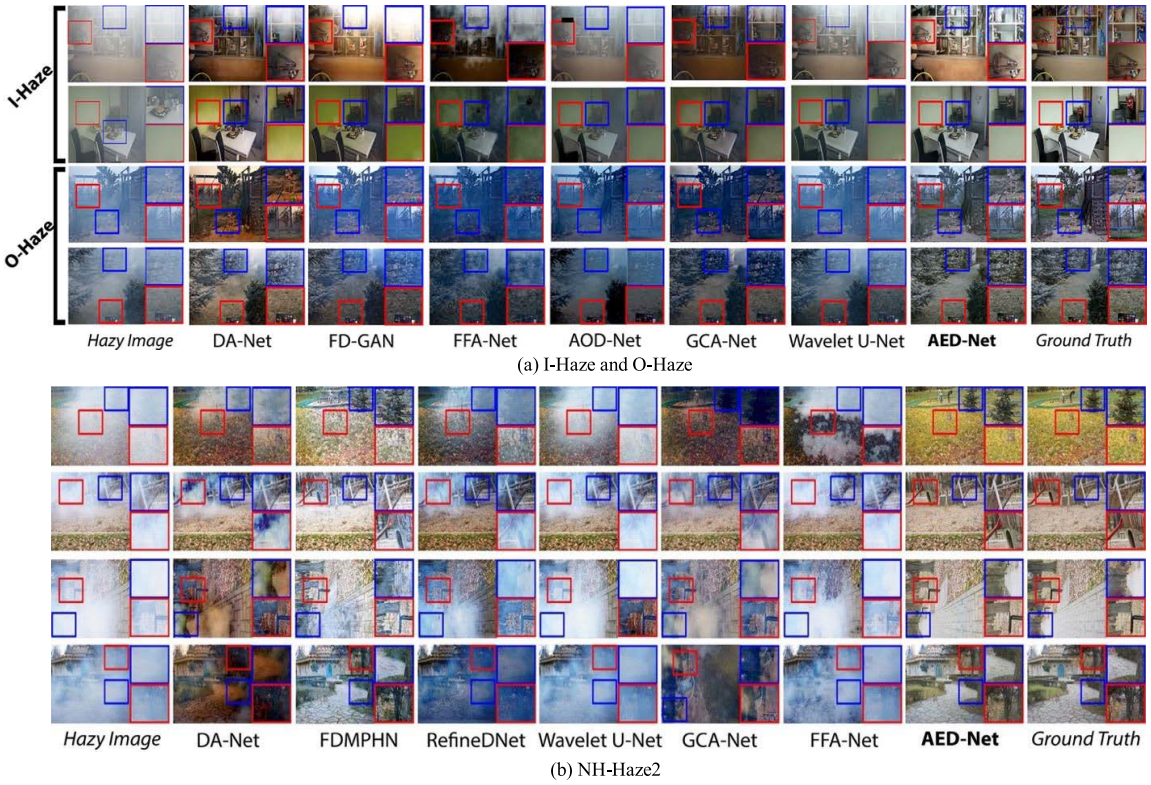

FIGURE 6. Qualitative comparisons of AED-Net on I/O-Haze (a) and NH-Haze2 (b) datasets.

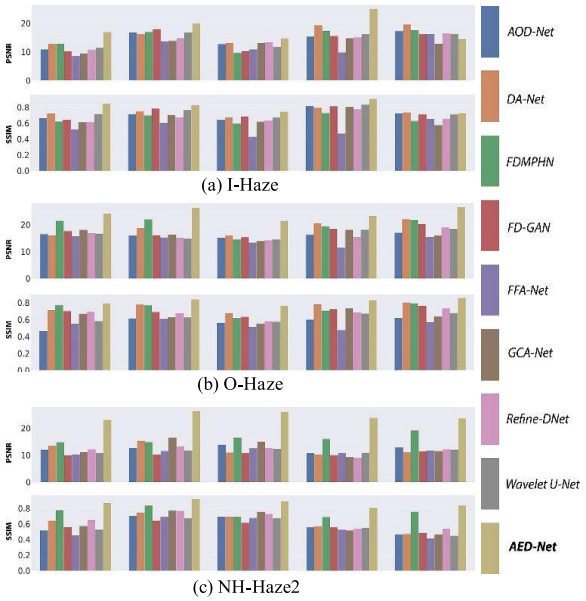

FIGURE 7. Comparison of AED-Net with other methods on individual images from I-Haze (a), O-Haze (b) and NH-Haze2 (c) datasets.

High PSNR, SSIM, FSIM, VIF, and low LPIPS scores indicate superior restoration compared to the ground truth. The perceptual similarity is an emergent property shared across deep visual representations [44]. Table 2 also shows the average and standard deviation values for each test dataset.

TABLE 3. Effectiveness of RAMGC module.

Datasets	I-Haze		O-Haze		NH-Haze2	
Metric	PSNR	SSIM	PSNR	SSIM	PSNR	SSIM
AED	20.52	0.865	25.20	0.845	24.30	0.854
AED + RAMGC	**20.75**	**0.872**	**25.56**	**0.845**	**24.64**	**0.863**

AED-Net generated the highest average values for all measures. The standard deviations are comparable with others. In addition, the PSNR and SSIM values for each image are provided in Fig.7. AED-Net has higher values for these two measures than other methods for almost all test images.

E. ABLATION STUDIES

To evaluate the contribution of the RAMGC module, we train the network with and without it. Table 3 displays the quantitative results on three datasets. It shows that utilizing RAMGC, an adaptive enhancement module, in the middle of the network achieves better PSNR and SSIM estimates. Fig. 8 (a) presents visual comparison of images with and without the RAMGC module. It also produces visually pleasing images. In addition, the significance of each block (Alpha, Beta, Gamma) is analyzed by iteratively removing each block (Fig 8 (b)). The computer simulations demonstrate that each block controls different image features, such as brightness, contrast, edges, etc. The combination of these blocks produces results closer to the ground truth.

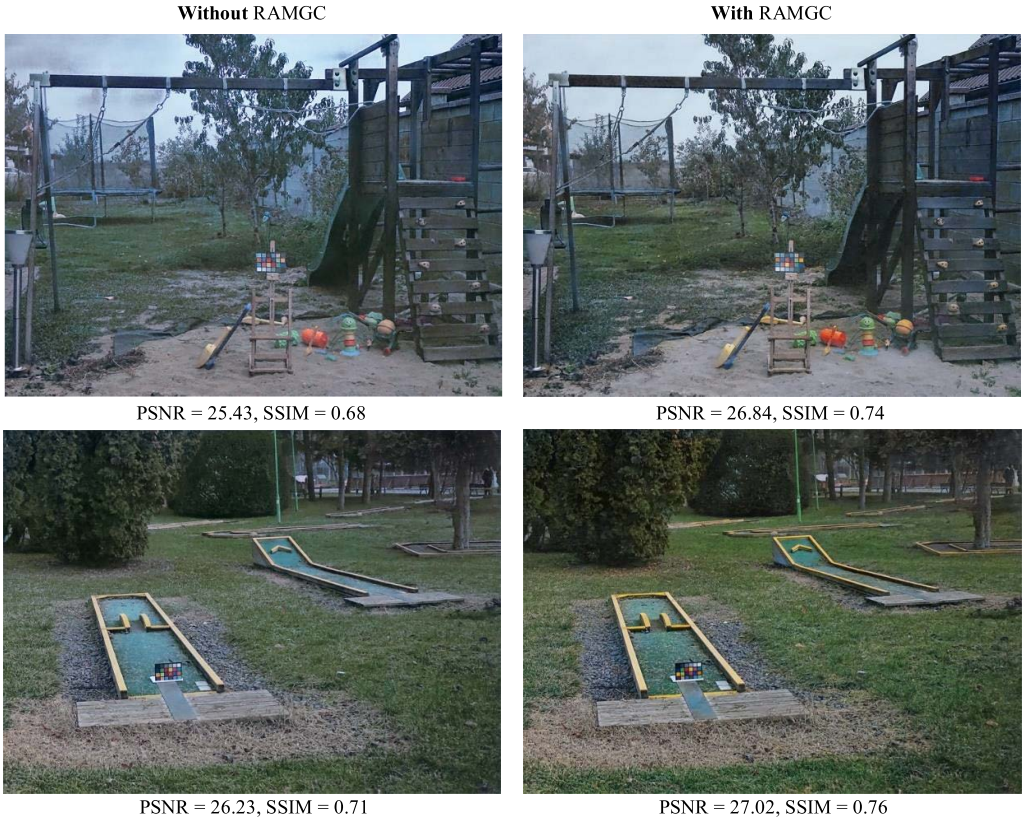

(a) Effectiveness of RAMGC Module

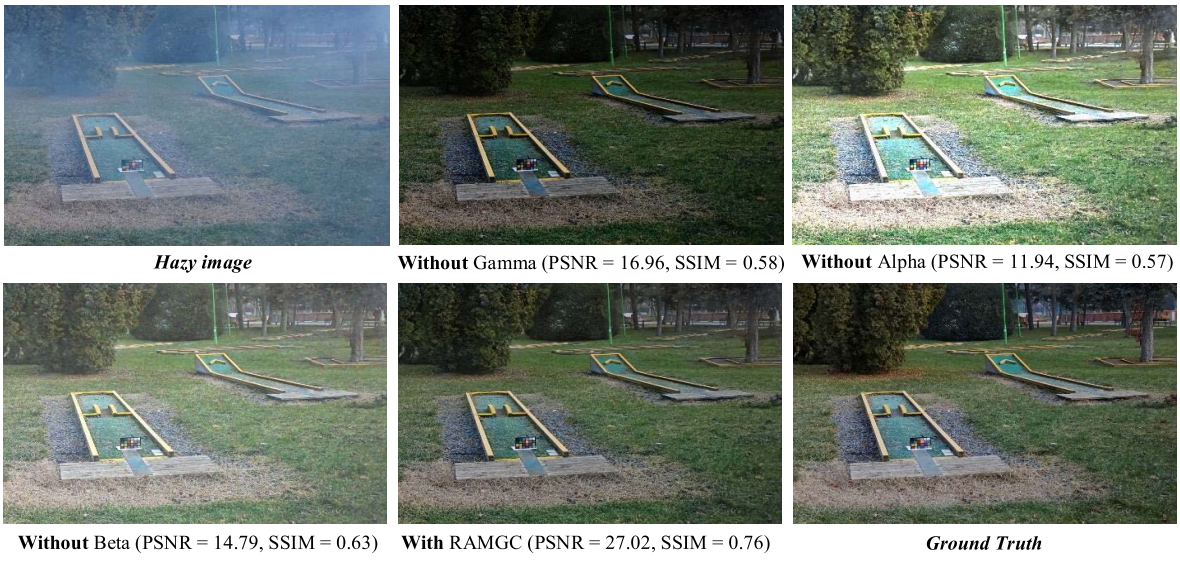

(b) Effectiveness of each block in RAMGC Module

FIGURE 8. **Qualitative and quantitative effectiveness of RAMGC module (a) and its submodules (b).**

F. CODALAB NTIRE 2021 NONHOMOGENEOUS IMAGE DEHAZING CHALLENGE

We have observed that virtually all methods struggle with nonhomogeneous haze. The Codalab NTIRE 2021 image dehazing challenge provides an extended version of the former NH-Haze dataset for the Codalab competition. The results of the nonhomogeneous dehazing challenge are reviewed, and proposed methods are evaluated in [27]. We compare AED-Net with the top-scoring methods which provide publicly available code. ADN dehaze [45] is based on a novel generative adversarial network with a 2D discrete wavelet transform structure. A two-branch dehazing

TABLE 4. Quantitative comparison of AED-Net with Codalab competition 2021 challenge top methods.

	ADN	TBD	SRKTDN	AED-Net
PSNR	20.898	21.66	20.13	**24.65**
SSIM	0.844	0.843	0.803	**0.868**

network (TBD) [12] proposes a simple but effective approach for nonhomogeneous dehazing via ensemble learning. SRK-TDN [16] is based on Knowledge Transfer Dehazing Network and Trident Dehazing Network. They propose a model with super-resolution and knowledge transfer methods. As shown in Table 4, AED-Net outperforms these three methods on the NH-Haze2 dataset in terms of PSNR and SSIM values.

IV. CONCLUSION

We propose a novel end-to-end adaptive enhancement dehazing network called AED-Net for single-image dehazing. It consists of gray level dehazing (GLD) based on the Res2Net encoder and a two-branch decoder, a novel region-aware modified Gamma correction (RAMGC), and a residual channel attention network (RCAN) that effectively combines high-level and low-level features. An ablation study demonstrated the effectiveness of the RAMGC module. Quantitative comparisons based on five key-metrics PNSR, SSIM, FSIM, VIF, and LPIPS, as well as qualitative analysis, were performed. The experimental results demonstrate that the proposed method outperforms state-of-the-art methods on benchmark datasets, real-world images, and the NH-Haze2 dataset of the Codalab NTIRE 2021 competition. We conclude that our novel RAMGC applied in conjunction with the two-branch treatment of haze contributes significantly to dehazing performance. We intend to explore dilated convolution with reduced parameters and verify the system's performance on other datasets for further research. Another promising area of future inquiry is combining the proposed model with the de-raining algorithm.

ACKNOWLEDGMENT

(Sargis A. Hovhannisyan and Hayk A. Gasparyan contributed equally to this work.)

REFERENCES

[1] Z. Liu, Y. He, C. Wang, and R. Song, "Analysis of the influence of foggy weather environment on the detection effect of machine vision obstacles," *Sensors*, vol. 20, no. 2, p. 349, Jan. 2020.

[2] E. J. McCartney, "Optics of the atmosphere: Scattering by molecules and particles," *Phys. Bull.*, vol. 28, no. 11, pp. 521–531, May 1977.

[3] S. K. Nayar and S. G. Narasimhan, "Vision in bad weather," in *Proc. 7th IEEE Conf. Comput. Vis.*, vol. 2, Sep. 1999, pp. 820–827.

[4] S. G. Narasimhan and S. K. Nayar, "Contrast restoration of weather degraded images," *IEEE Trans. Pattern Anal. Mach. Learn.*, vol. 25, no. 6, pp. 713–724, Jun. 2003.

[5] Y. Schechner, S. G. Narasimhan, and S. K. Nayar, "Instant dehazing of images using polarization," *Proc. IEEE Comput. Soc. Conf. Comp. Vis. Pattern Recognit.*, vol. 1, Dec. 2001, pp. 325–332.

[6] S. Shwartz, E. Namer, and Y. Y. Schechner, "Blind haze separation," in *Proc. IEEE Comput. Soc. Conf. Comput. Vis. Pattern Recognit.*, vol. 2, Jun. 2006, pp. 1984–1991.

[7] B. Li, X. Peng, Z. Wang, J. Xu, and D. Feng, "AOD-Net: All-in-one dehazing network," in *Proc. IEEE Int. Conf. Comput. Vis. (ICCV)*, Oct. 2017, pp. 4770–4778.

[8] D. Chen, M. He, Q. Fan, J. Liao, L. Zhang, D. Hou, L. Yuan, and G. Hua, "Gated context aggregation network for image dehazing and deraining," in *Proc. IEEE Winter Conf. Appl. Comput. Vis. (WACV)*, Jan. 2019, pp. 1375–1383.

[9] X. Qin, Z. Wang, Y. Bai, X. Xie, and H. Jia, "FFA-Net: Feature fusion attention network for single image dehazing," in *Proc. AAAI Conf. Artif. Intell.*, 2020, pp. 11908–11915.

[10] Y. Shao, L. Li, W. Ren, C. Gao, and N. Sang, "Domain adaptation for image dehazing," in *Proc. IEEE/CVF Conf. Comput. Vis. Pattern Recognit. (CVPR)*, Jun. 2020, pp. 2808–2817.

[11] S. D. Das and S. Dutta, "Fast deep multi-patch hierarchical network for nonhomogeneous image dehazing," in *Proc. IEEE/CVF Conf. Comput. Vis. Pattern Recognit. Workshops (CVPRW)*, Jun. 2020, pp. 482–483.

[12] Y. Yu, H. Liu, M. Fu, J. Chen, X. Wang, and K. Wang, "A two-branch neural network for non-homogeneous dehazing via ensemble learning," in *Proc. IEEE/CVF Conf. Comput. Vis. Pattern Recognit. Workshops (CVPRW)*, Jun. 2021, pp. 193–202.

[13] Y. Dong, Y. Liu, H. Zhang, S. Chen, and Y. Qia, "FD-GAN: Generative adversarial networks with fusion-discriminator for single image dehazing," in *Proc. AAAI Conf. Artif. Intell.*, Apr. 2020, pp. 10729–10736.

[14] S. Zhao, L. Zhang, Y. Shen, and Y. Zhou, "RefineDNet: A weakly supervised refinement framework for single image dehazing," *IEEE Trans. Image Process.*, vol. 30, pp. 3391–3404, 2021.

[15] H.-H. Yang and Y. Fu, "Wavelet U-Net and the chromatic adaptation transform for single image dehazing," in *Proc. IEEE Int. Conf. Image Process. (ICIP)*, Sep. 2019, pp. 2736–2740.

[16] T. Chen, J. Fu, W. Jiang, C. Gao, and S. Liu, "SRKTDN: Applying super resolution method to dehazing task," in *Proc. IEEE/CVF Conf. Comput. Vis. Pattern Recognit. Workshops (CVPRW)*, Jun. 2021, pp. 487–496.

[17] M. Ju, C. Ding, D. Zhang, and Y. J. Guo, "Gamma-correction-based visibility restoration for single hazy images," *IEEE Signal Process. Lett.*, vol. 25, no. 7, pp. 1084–1088, Jul. 2018.

[18] R. T. Tan, "Visibility in bad weather from a single image," in *Proc. IEEE Conf. Comput. Vis. Pattern Recognit.*, Jun. 2008, pp. 1–8.

[19] K. He, J. Sun, and X. Tang, "Single image haze removal using dark channel prior," *IEEE Trans. Pattern Anal. Mach. Intell.*, vol. 33, no. 12, pp. 2341–2353, Dec. 2011.

[20] S. Huang, Y. Liu, Y. Wang, Z. Wang, and J. Guo, "A new haze removal algorithm for single urban remote sensing image," *IEEE Access*, vol. 8, pp. 100870–100889, 2020.

[21] E. H. Land and J. J. McCann, "Lightness and retinex theory," *J. Opt. Soc. Amer.*, vol. 61, no. 1, p. 1, 1971.

[22] A. M. Chaudhry, M. M. Riaz, and A. Ghafoor, "A framework for outdoor RGB image enhancement and dehazing," *IEEE Geosci. Remote Sens. Lett.*, vol. 15, no. 6, pp. 932–936, Jun. 2018.

[23] J. Gui, X. Cong, Y. Cao, W. Ren, J. Zhang, J. Zhang, and D. Tao, "A comprehensive survey on image dehazing based on deep learning," in *Proc. Int. Joint Conf. Artif. Intell.*, Aug. 2021, pp. 1–8.

[24] B. Cai, X. Xu, K. Jia, C. Qing, and D. Tao, "DehazeNet: An end-to-end system for single image haze removal," *IEEE Trans. Image Process.*, vol. 25, no. 11, pp. 5187–5198, Nov. 2016.

[25] A. S. Parihar, Y. K. Gupta, Y. Singodia, V. Singh, and K. Singh, "A comparative study of image dehazing algorithms," in *Proc. 5th Int. Conf. Commun. Electron. Syst. (ICCES)*, Jun. 2020, pp. 766–771.

[26] J. Liu, S. Wang, X. Wang, M. Ju, and D. Zhang, "A review of remote sensing image dehazing," *Sensors*, vol. 21, no. 11, p. 3926, Jan. 2021.

[27] C. O. Ancuti *et al.*, "NTIRE 2021 nonhomogeneous dehazing challenge report," in *Proc. IEEE/CVF Conf. Comput. Vis. Pattern Recognit. Workshops (CVPRW)*, Jun. 2021, pp. 627–646.

[28] S.-H. Gao, M.-M. Cheng, K. Zhao, X.-Y. Zhang, M.-H. Yang, and P. Torr, "Res2Net: A new multi-scale backbone architecture," *IEEE Trans. Pattern Anal. Mach. Intell.*, vol. 43, no. 2, pp. 652–662, Feb. 2021.

[29] Y. Zhang, K. Li, K. Li, L. Wang, B. Zhong, and Y. Fu, "Image super-resolution using very deep residual channel attention networks," in *Proc. Eur. Conf. Comp. Vis. (ECCV)*, Jul. 2018, pp. 286–301.

[30] C. O. Ancuti, C. Ancuti, R. Timofte, and C. De Vleeschouwer, "O-HAZE: A dehazing benchmark with real hazy and haze-free outdoor images," in *Proc. IEEE/CVF Conf. Comput. Vis. Pattern Recognit. Workshops (CVPRW)*, Jun. 2018, pp. 754–762.

[31] C. O. Ancuti, C. Ancuti, R. Timofte, and C. De Vleeschouwer, "O-HAZE: A dehazing benchmark with real hazy and haze-free outdoor images," in *Proc. IEEE/CVF Conf. Comput. Vis. Pattern Recognit. Workshops (CVPRW)*, Jun. 2018, pp. 620–631.
[32] W. Shi, J. Caballero, F. Huszar, J. Totz, A. P. Aitken, R. Bishop, D. Rueckert, and Z. Wang, "Real-time single image and video super-resolution using an efficient sub-pixel convolutional neural network," in *Proc. IEEE Conf. Comput. Vis. Pattern Recognit. (CVPR)*, Jun. 2016, pp. 1874–1883.
[33] C. X. Liu, J. W. Zhao, Y. Y. Shen, Y. G. Zhou, X. Wang, and Y. Ouyang, "Texture filtering based physically plausible image dehazing," *Vis. Comput.*, vol. 32, nos. 6–8, pp. 911–920, 2016.
[34] Y. Qu, Y. Chen, J. Huang, and Y. Xie, "Enhanced pix2pix dehazing network," in *Proc. IEEE/CVF Conf. Comput. Vis. Pattern Recognit. (CVPR)*, Jun. 2019, pp. 8160–8168.
[35] R. Girshick, "Fast R-CNN," in *Proc. IEEE Int. Conf. Comput. Vis. (ICCV)*, Dec. 2015, pp. 1440–1448.
[36] J. Johnson, A. Alahi, and L. Fei-Fei, "Perceptual losses for real-time style transfer and super-resolution," in *Proc. Eur. Conf. Comput. Vis. (ECCV)*, 2016, pp. 694–711.
[37] K. Simonyan and A. Zisserman, "Very deep convolutional networks for large-scale image recognition," in *Proc. Int. Conf. Learn. Represent. (ICLR)*, 2015, pp. 1–14.
[38] T. Trongtirakul, W. Chiracharit, and S. S. Agaian, "Single backlit image enhancement," *IEEE Access*, vol. 8, pp. 71940–71950, 2020.
[39] C. Ledig, L. Theis, F. Huszar, J. Caballero, A. Cunningham, A. Acosta, A. Aitken, A. Tejani, J. Totz, Z. Wang, and W. Shi, "Photo-realistic single image super-resolution using a generative adversarial network," in *Proc. IEEE Conf. Comput. Vis. Pattern Recognit. (CVPR)*, Jul. 2017, pp. 4681–4690.
[40] C. O. Ancuti, C. Ancuti, and R. Timofte, "NH-HAZE: An image dehazing benchmark with non-homogeneous hazy and haze-free images," in *Proc. IEEE/CVF Conf. Comput. Vis. Pattern Recognit. Workshops (CVPRW)*, Jun. 2020, pp. 1798–1805.
[41] Z. Wang, A. C. Bovik, H. R. Sheikh, and E. P. Simoncelli, "Image quality assessment: From error visibility to structural similarity," *IEEE Trans. Image Process.*, vol. 13, no. 4, pp. 600–612, Apr. 2004.
[42] L. Zhang, L. Zhang, X. Mou, and D. Zhang, "FSIM: A feature similarity index for image quality assessment," *IEEE Trans. Image Process.*, vol. 20, no. 8, pp. 2378–2386, Aug. 2011.
[43] H. R. Sheikh and A. C. Bovik, "Image information and visual quality," *IEEE Trans. Image Process.*, vol. 15, no. 2, pp. 430–444, Feb. 2006.
[44] R. Zhang, P. Isola, A. A. Efros, E. Shechtman, and O. Wang, "The unreasonable effectiveness of deep features as a perceptual metric," in *Proc. IEEE/CVF Conf. Comput. Vis. Pattern Recognit.*, Jun. 2018, pp. 586–595.
[45] M. Fu, H. Liu, Y. Yu, J. Chen, and K. Wang, "DW-GAN: A discrete wavelet transform GAN for nonhomogeneous dehazing," in *Proc. IEEE/CVF Conf. Comput. Vis. Pattern Recognit. Workshops (CVPRW)*, Jun. 2021, pp. 203–212.
[46] K. Panetta, C. Gao, and S. Agaian, "No reference color image contrast and quality measures," *IEEE Trans. Consum. Electron.*, vol. 59, no. 3, pp. 643–651, Aug. 2013.
[47] K. Panetta, A. Samani, and S. Agaian, "A robust no-reference, no-parameter, transform domain image quality metric for evaluating the quality of color images," *IEEE Access*, vol. 6, pp. 10979–10985, 2018.
[48] J. Liu, W. Liu, J. Sun, and T. Zeng, "Rank-one prior: Toward real-time scene recovery," in *Proc. IEEE/CVF Conf. Comput. Vis. Pattern Recognit.*, Apr. 2021, pp. 14802–14810.
[49] W. Ren, L. Ma, J. Zhang, J. Pan, X. Cao, W. Liu, and M.-H. Yang, "Gated fusion network for single image dehazing," in *Proc. IEEE/CVF Conf. Comput. Vis. Pattern Recognit.*, Jun. 2018, pp. 3253–3261.
[50] Q. Yi, J. Li, Q. Dai, F. Fang, G. Zhang, and T. Zeng, "Structure-preserving deraining with residue channel prior guidance," in *Proc. IEEE/CVF Int. Conf. Comput. Vis.*, Oct. 2021, pp. 4238–4247.
[51] K. Lakhwani, P. D. Murarka, and N. S. Chauhan, "Color space transformation for visual enhancement of noisy color image," *IET Image Process.*, vol. 3, no. 2, pp. 9–11, 2015.

SARGIS A. HOVHANNISYAN received the bachelor's degree in informatics and applied mathematics from Yerevan State University, Armenia, in 2020. He is currently pursuing the master's degree in data science. His primary research interests are computer vision, deep learning, and artificial intelligence.

HAYK A. GASPARYAN received a bachelor's degree in informatics and applied mathematics from Yerevan State University, Armenia, in 2020. He is currently pursuing the master's degree in data science. His primary research interests are computer vision, deep learning, and artificial intelligence.

SOS S. AGAIAN (Fellow, IEEE) is currently a Distinguished Professor with the College of Staten Island (CSI), City University of New York. He has authored more than 750 technical articles and ten books in his research areas. The technologies that he invented have been adopted by multiple institutions, including the U.S. Government, and commercialized by industry. His current research focuses on computational vision, artificial intelligence, multimedia security, multimedia analytics, and biologically inspired signal/image processing modeling. He is a fellow of SPIE, IS&T, AAAS, and AAIA. He is a Foreign Member of the Armenian National Academy. He was a recipient of the Distinguished Research Award from The University of Texas at San Antonio, the Innovator of the Year Award, in 2014, and the Tech Flash Titans-Top Researcher Award (*San Antonio Business Journal*). He received several best paper awards. He is the co-founder of three university Centers. He is currently an Associate Editor of the IEEE TRANSACTIONS ON IMAGE PROCESSING, the IEEE TRANSACTIONS ON SYSTEMS, MAN, AND CYBERNETICS, and the *Journal of Electronic Imaging* (IS&T and SPIE). He gave more than 20 plenary/keynote speeches and more than 50 invited talks.

ART GHAZARYAN received the Diploma degree (Hons.) in electrical engineering from Yerevan State University, the M.A. degree in telecommunications from Ohio University, the M.S. degree in computer science from Tufts University, and the Sloan Fellow M.B.A. from the Massachusetts Institute of Technology.